scientific reports

Check for updates

OPEN

Effects of mandrel velocity on residual stresses created in cold expansion process of adjacent holes for AA6016-T6 and AA1100 aluminum alloys

Saeed Yaghoubi[1]✉ & Ali Shirazi[2]

Cold expansion is a mechanical method for creating residual stresses. This method is a proven technique to increase the fatigue life, and checking the residual stress on it, is of particular importance. A cold expansion process is widely used to generate beneficial residual stresses into an annular region around the hole. In the present research work, AA 6016-T6 and AA 1100 aluminum alloys which are two strain rate sensitive materials, were subjected to cold expansion process with different mandrel velocities. In fact, the effect of mandrel velocity on the created residual stresses has been investigated. The constants of the Johnson-Cook material model have been determined for them and the process has been investigated, experimentally and numerically. The obtained results revealed that the values of the residual stresses created in the sheets depend on the velocity of the process especially at the edge of the sheets holes. By increasing the mandrel velocity from 5 to 500 mm/min, depending on the distance from the hole to the edge of the sheet, it is possible to enhance the hoop residual stress by 37.3–41.2% in AA 1100 aluminum alloy and by 37.6–38.1% in AA 6016-T6 aluminum alloy. This research showed that in all cases, the radial residual stresses created around the holes are negative. Also, it was cleared that due to the existence of material constraints and the movement of the sheet material, the amount of hoop residual stress created in the mid-thickness is more than the exit face and in the exit face is also more than the entrance face, exactly unlike the size of their zones.

Keywords Cold expansion, Residual stress, Johnson-Cook model, Strain rate, Finite element

In many cases, the holes created in the sheets for using of pins[1], rivets[2] and bolts[3] are subjected to fatigue loading, which is more evident in the aerospace[4] and automotive[5] industries. This fatigue loading causes the sheet to failure in the holes location. To prevent this problem, solutions such as fastener interference fitting[6,7], bolt clamping[8] and Cold Expansion (CE)[2,9,10] have been proposed, which are widely employed to avoid reducing the fatigue life of the sheets. In the CE process, a mandrel with a diameter slightly larger than the diameter of the sheet hole enters the sheet with the force of the press and exits from the other side, so as to create compressive residual stresses around the sheet hole and increase its fatigue life[11]. Based on this, the study of residual stress in such processes is of particular importance[12–15]. Residual stresses have a significant influence on the behavior of materials. Also, if a workpiece is to be produced in several stages, the residual stresses created in each stage will affect the next stages of production[16]. Residual stresses have a remarkable effect on the mechanical behavior of materials in which they are supported, as has been reported in a number of recent works. Residual stresses are important and decisive factors. For example, these factors can have damaging consequences when generated in components during the manufacturing process. On the other hand, residual stresses can improve the properties of structures (for example, in pre-stressed car windscreens)[17]. In the present study, the cold expansion process was carried out on AA 1100 aluminum and AA 6016-T6 aluminum alloys. The reason for choosing these two aluminums is their wide applications. AA 1100 aluminum alloy sheet is used in light weight structures[18], transportation industry and train wagons[19], aerospace[20] and automotive industries[21], low pressure panels, heat exchangers and general sheeting[22]. Also, AA 6016-T6 aluminum alloy is employed in aerospace, defense, marine

[1]Department of Mechanical Engineering, Faculty of Engineering, Ilam University, Ilam, Iran. [2]Department of Mechanical Engineering, Faculty of Engineering, Bu-Ali Sina University, Hamedan, Iran. ✉email: S.yaghoubi@ilam.ac.ir

and weapon manufacturing industries[23]. These sheets are also used in the automotive industry[24], making bicycle bodies, and motor boats[25].

Several researches have been carried out in the field of cold expansion process by researchers. Gattmah et al.[26] experimentally and numerically investigated the cold tube drawing process on AISI 1010 steel tube. For this purpose, they used a fixed mandrel and studied the generated residual stresses. They considered two different reductions of areas of 16% and 23% and used X-ray diffraction (XRD) method to determine the hoop residual stresses inside the tube wall at five different orientations. They concluded that although the reduction of area strongly affects the residual stress compared to other process parameters, the friction coefficient has minimum effect on residual stresses. Also, the residual stress states inside the tube wall produced by cylindrical and conical plugs are completely different. In another study, Gattmah et al.[27] investigated the residual stresses created in DIN 17,100 St 37–2 steel tubes produced by floating plug drawing process. In their research, the influences of various tool parameters such as plug half angle, cone half angle of the die, fillet radius of the plug, and fillet radius of the die on the induced residual stresses were investigated using FEM. They found that there is a good convergence between the experimental and numerical findings with slight differences in the values. On the other hand, the FEM results revealed that the plug half angle at 0° and the cone half angle of the die at 9° induce the minimum residual stresses compared to other angles. Geng et al.[28] focused on fatigue performance improvement in AZ31 blank assisted by electromagnetic cold expansion process. According to their results, a good surface integrity and grain refinement around the hole for the workpiece treated by aforementioned operation was achieved. Pucillo et al.[29] analyzed the CE process on the holes of the railway rails. These rails are made of R260 rail steel. They applied two levels of expansion to this steel and investigated the effect of this process on the resistance to fatigue crack growth of the metal. They revealed that when the diameter interference is 2%, the amount of resistance to fatigue crack growth enhances from 50 to 100% and when the diameter interference is 4%, this quantity increases to 200%. Faghih et al.[30] conducted the CE process on the rolled AZ31B magnesium alloy at the level of 6%. Then, they compared the fatigue life of processed samples with the fatigue life of other specimens and found that the fatigue life of these samples was significantly improved. As an example, the endurance limit of the processed samples was equal to 150 MPa, while the endurance limit of other samples was equal to 80 MPa. This research also showed that carrying out the CE process can not only delay the formation of cracks, but also slow down its growth rate. In another study, Gattmah et al.[31] developed a new measurement technique for residual stresses generated by the cold tube drawing process with a fixed mandrel. This new development of measurement technique that is built on the removing layer method is employed to measure the axial and the hoop residual stresses inside the tube wall for AISI 1010 steel. Additionally, they were performed an axisymmetric finite element model based on explicit dynamic analysis to predict the mentioned stresses within tube thickness. By conducting this study, it was cleared that the results are in good agreement and the new measurement technique is proved to be one of the appropriate methods to measure residual stresses inside the tube wall. Moreover, their findings showed that the residual stresses present inside the tube wall are completely different by different reduction of areas of $R = 16\%$ and 23%. Su et al.[32] performed the CE process on 7075-T651 aluminum alloy plate and investigated its effects on this plate. It was cleared that carrying out this process causes a significant plastic deformation in the on 7075-T651 aluminum alloy plate, and as a result, its microstructure improves. Due to this microstructure improvement, the hardness of the plate also increases and therefore its fatigue behavior is also improved.

Based on the observations made, it can be said that no comprehensive research has been done on the cold expansion process and the calculation of the resulting residual stress. In the present study, AA 6016-T6 aluminum and AA 1100 aluminum alloys were subjected to cold expansion process. For this purpose, different mandrel velocities were employed. In these processes, radial and hoop stress values were determined experimentally using strain gauges. Afterwards, the conducted experiments were simulated and the accuracy of the simulations was ensured by comparing the results of the simulation and the experimental outcomes. The distribution of residual stresses around the holes of the sheets was determined for different mandrel velocities. Also, the distributions of stress in the circumferential or tangential directions and in the entrance face, the exit face, and mid-thickness were determined and compared, comprehensively. The novelty of this research can be summarized as bellows:

- Investigating the effects of the simultaneous entry of two identical mandrels into two adjacent holes from a plate and their passing through these holes at the same velocity but at several different velocity ranges, on the residual stresses created in the plate.
- Experimental determination of the Johnson-Cook parameters for AA 6016-T6 and AA 1100 aluminum alloys due to sensitivity of the material model to strain rate in the numerical simulation of the cold expansion process.

Materials and methods

Materials

The materials chosen for the CE process in current research are AA 6016-T6 and AA 1100 aluminum alloys. The chemical composition of these alloys are presented in the Table 1.

The dog-bone shaped tensile test specimens were cut and made from the two mentioned aluminum alloys to obtain the stress-strain graphs and tensile properties, according to ASTM E8 standard[16]. The dimensions of this standard samples is shown in Fig. 1.

In the present research work, Johnson-Cook material model is used for numerical simulations. Therefore, in addition to tensile properties, the parameters of this material model should be determined using tensile tests with appropriate conditions for both AA 6016-T6 and AA 1100 alloys. For this purpose, three groups of tensile tests were conducted. The first group was related to the simple tensile tests that were performed with the 15-Tons SANTAM machine to determine the material's stress-strain diagrams at room temperature. The second category

Material	Al	Be	Cu	Mn	Zn	Si	Fe	Mg	Ti
AA 6016-T6	Balance	0.0005	0.05	0.03	0.07	0.04	0.07	–	–
AA 1100	Balance	–	0.004	0.007	0.005	1.2	0.17	0.3	0.01

Table 1. Chemical composition (wt%) of AA 6016-T6 and AA 1100 alloys used in present study.

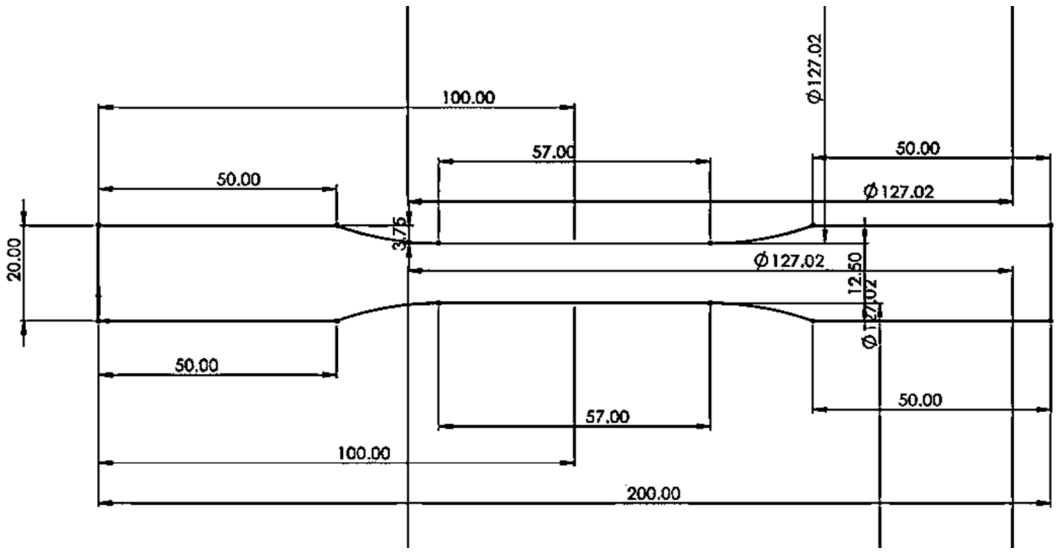

Fig. 1. Dog-bone shaped tensile test specimen according to ASTM E8.

was corresponded to the tensile tests that were conducted with the same machine at different high temperatures in order to determine the temperature-related parameter in the Johnson-Cook material model. In this case, an electrical furnace was installed on the SANTAM machine. Finally, the third group was the tensile tests that were performed at different velocities to determine the parameter related to the strain rate in the material model for both AA 6016-T6 and AA 1100 alloys.

Cold expansion process

To carry out the cold expansion processes, AA 6016-T6 and AA 1100 aluminum sheets were prepared. The dimensions of these workpiece are shown in Fig. 2. The thickness of the sheets, the diameter of the holes, and the distance between the centers of the holes are considered to 3 mm, 8 mm, and 20 mm, respectively. In order to validate the simulation results, the hoop and radial residual strains along two lines around the holes were experimentally measured. One of these lines is considered horizontally next to the one of the holes and the other line is vertically next to the other hole. These two lines, namely line 1 and line 2, are also shown in Fig. 2. To measure the strain on these lines, the rosette strain gauges with an angle of 45 degrees have been employed. These strain gauges are attached to line 1 and line 2 as shown in mentioned figure.

Two completely similar mandrels have been used to carry out the CE processes in current research. During the CEP, these two mandrels entered the sheet holes at the same time and passed through them at the same velocity, simultaneously. The material of mandrels is CK45 steel with hardness of Rockwell C 215, yield stress of 470 MPa, ultimate tensile strength of 660 MPa, and Poisson ratio of 0.29. The relevant studies show that the better outcomes are obtained in the case of simultaneous insertion of two mandrels into the sheet holes compared to their sequential penetration. In the superior state, the sheet will be more resistant to fatigue loading. The reason for this observation is that at the same time, more residual stress is induced to the sheet. To investigate the effect of mandrel velocity on the residual stresses created in the sheet, the mandrels were passed through the holes at different velocities and the amounts of strain that the strain gauges showed in the hoop and radial direction on line 1 and line 2 were recorded. Then, the values of residual stresses were calculated based on these strains. The image of one of the two mandrels and its dimensions is shown in Fig. 3. The maximum diameter of mandrel is 8.32 mm and realizes 4% of CE. This diametric interference is calculated using Eq. (1)[33].

$$e = \frac{d - D}{D} \times 100\% \tag{1}$$

In Eq. (1), e is the diametric interference, and d and D are the maximum diameter of mandrel and the diameter of sheet hole, respectively.

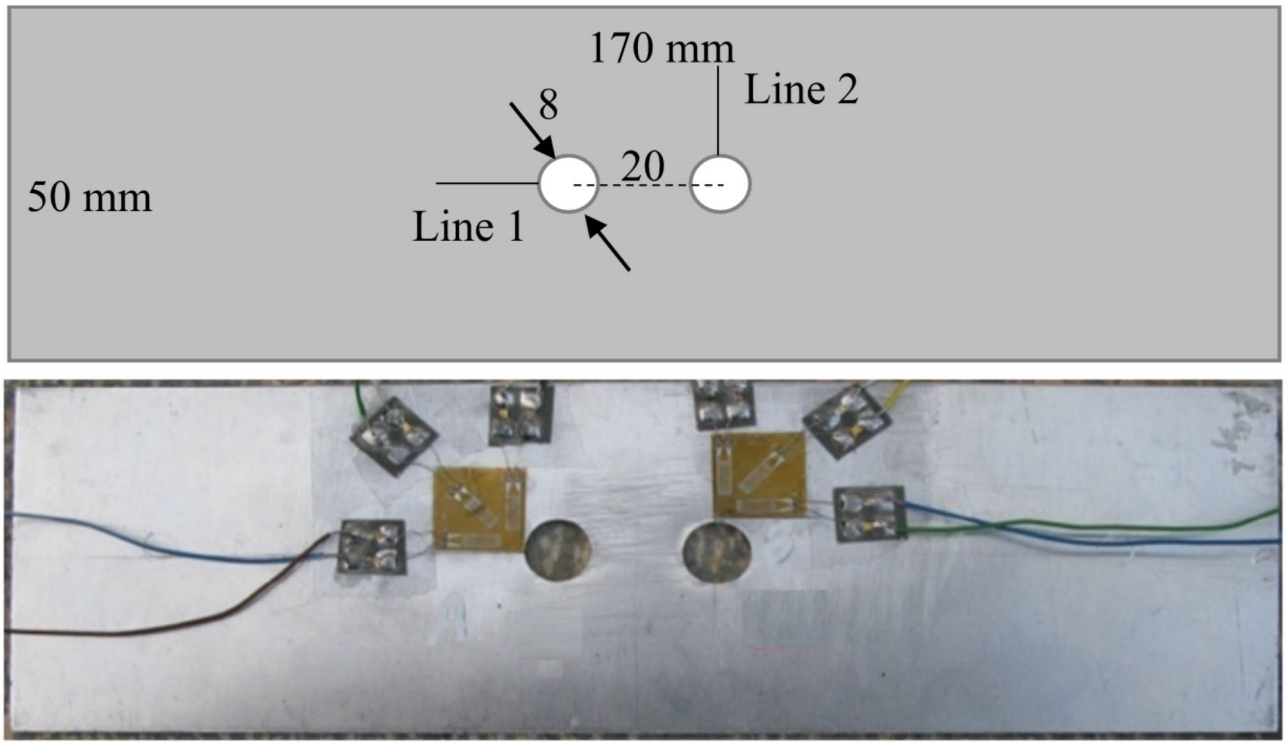

Fig. 2. Rosette strain gauge attached on the line 1 and line 2 in prepared specimen (dimensions in mm).

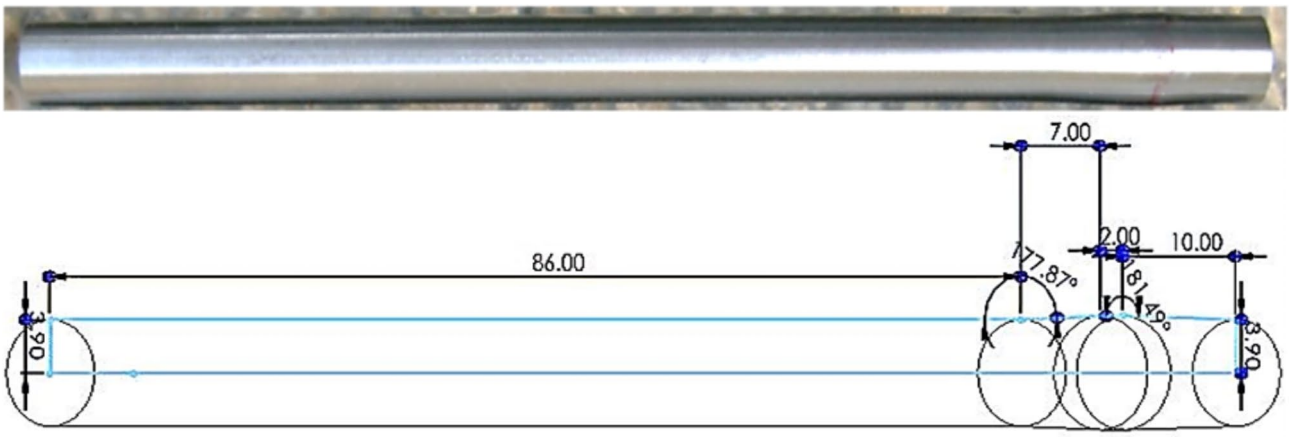

Fig. 3. The mandrel employed in current study and its dimensions (in millimeter).

Numerical simulation of CE process

The numerical simulations of CE process were carried out using LS-Dyna hydro code. This simulator software can model many processes well, especially those that depend on the time. Due to the symmetries in the geometry and loading of the present problem, it is enough to model only a quarter of the problem parts. Mandrel and sheet models that are simulated as a quarter are shown in Fig. 4.

In order to model the 1/4 of the blank sheet and mandrel, 28,800 and 1920 elements with eight-node linear brick specifications were used, respectively. According to Fig. 2, the dimensions of 1/4 of the sheet model are 50 × 85 mm, and the thickness of sheet is considered to 3 mm. In the LS-Dyna software, there is an option called "Bias" which can be used to produce meshes of different sizes in a part. Therefore, by using this option, the elements of the sheet that are near the holes are created fine and small in comparison with the regions far from the hole. That's why the accuracy of the solution can be increased and the required processing time is reduced. The volume of each of the modeled parts can be easily determined with the help of LS-Dyna software. Based on this, the volume of the 1/4 of the blank sheet is 6299.91 mm^3 and the volume of the 1/2 of the mandrel is 1191.91 mm^3. Therefore, the average sizes of sheet and mandrel elements are considered to, in turn, 0.2187 mm^3 and 0.6208 mm^3. Of course, as you get closer to the hole of sheet, the size of the elements becomes smaller, and

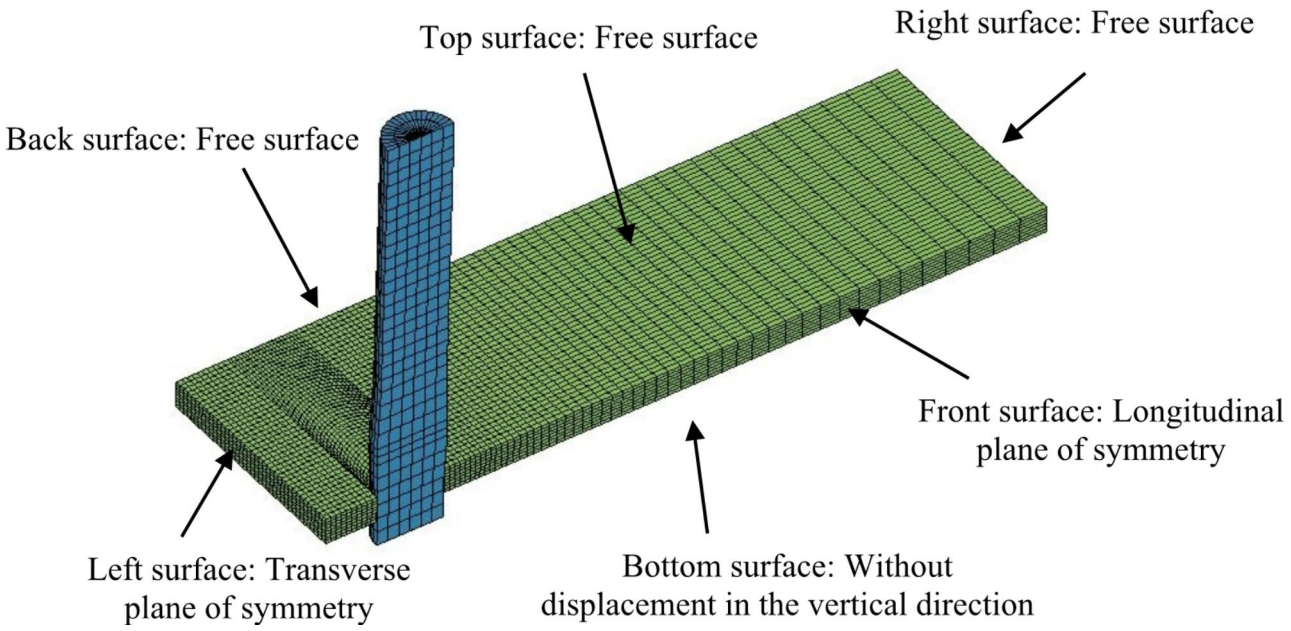

Fig. 4. The mandrel and sheet models in LS-Dyna.

around the hole, the size of the element is approximately considered to 0.1247 mm^3. The mandrel is eliminated as a rigid body and its elements are only allowed to move in the direction perpendicular to the sheet and along the sheet hole. Limiting the movement of sheet elements is also the definition of two planes of symmetry and the inclusion of a rigid wall below it to prevent it from moving downwards. This rigid wall has a hole created in front of the sheet hole.

The contact (interaction) type between the workpiece and the mandrel is defined as "contact_automatic_surface_to_surface". The friction coefficient between the mandrel and sheet which are made of steel and aluminum is considered as 0.3[34]. The friction model considered in this simulation is the Coulomb friction model (τ_f=$\mu\sigma_n$), where τ_f and σ_n are the friction shear stress and the normal stress between the workpiece and the mandrel surfaces, respectively. The Johnson-Cook material model is employed to workpiece, whose parameters are experimentally obtained in the present research for the two used materials. The mandrel is also considered rigid and the rigid material model is considered for it. In the performed simulations, the mandrel was passed through the specimen at the same velocities as it passes through the sheet hole in the experiment. The results obtained from these simulations are presented in Sect "Cold expansion process results" and validated using experimental findings.

Results and discussions

Johnson-Cook material model parameters

The Johnson-Cook material model, regarding the influence of strain hardening, the strain rate of the material and the effect of its softening, is considered as one of the most widely employed models to determine the plastic behavior of the material during the numerical simulation process[35]. The general form of the Johnson-Cook material model is presented in Eq. (2)[36]. In this equation, *A*, *B*, *C*, *n* and *m* are the constants of the material, which are determined from the tensile tests.

$$\sigma = (A + B(\bar{\varepsilon})^n)\,(1 + CLn\dot{\bar{\varepsilon}})\,(1 - T^{*m}) \tag{2}$$

Also, $\bar{\varepsilon}$ and $\dot{\bar{\varepsilon}}$are, in turn the equivalent plastic strain and the plastic strain rate, and T^* is the homologous temperature. The last quantity is defined using Eq. (3).

$$T^* = \frac{T - T_{room}}{T_{melt} - T_{room}} \tag{3}$$

where, T_{room} and T_{melt} are the room temperature and melting temperature, and their values are considered to 27°C and 660℃, respectively. The true stress-strain curves of aluminum alloys used in present research are shown in Fig. 5. These curves, which are determined by performing the experiments mentioned in Sect "Materials", can be directly used to determine A, B, and n constants. In fact, A is yield stress and by transferring the coordinate origin to the yield point on the stress-strain diagram and fitting an exponential curve on the plastic part of it, *B* and *n* can also be determined. Accordingly, *A*, *B*, and *n* for AA 6016-T6 are 291 MPa, 286 MPa and 0.63 and for AA 1100 are 78 MPa, 62 MPa and 0.42, respectively. As mentioned earlier, to determine the *C*- parameter, the tensile tests with different velocities were performed at room temperature ($T^* = 0$). Based on these practical

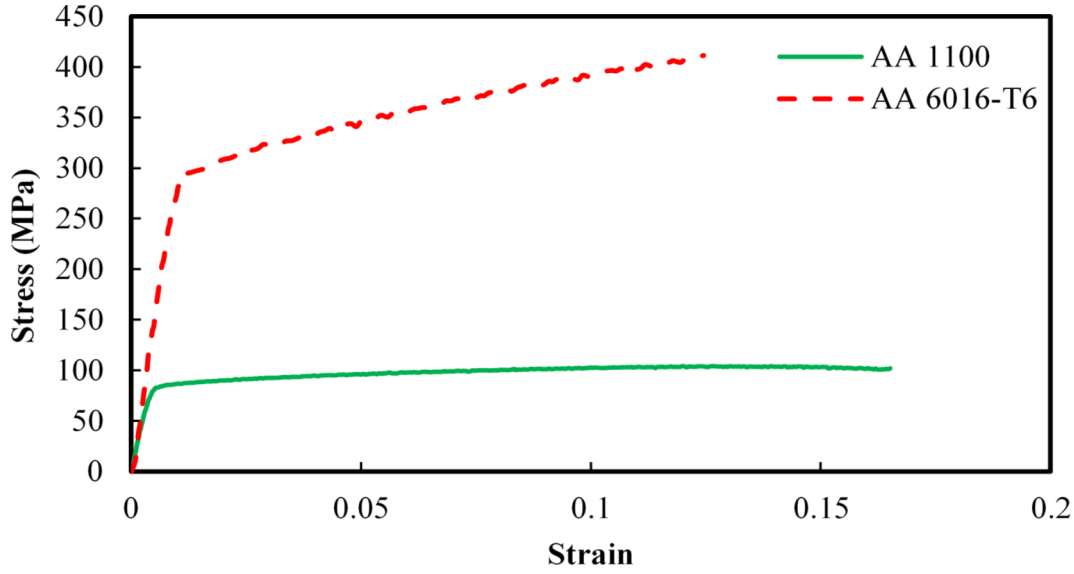

Fig. 5. True stress-strain curves of AA 1100 and AA 6016-T6 aluminum alloys.

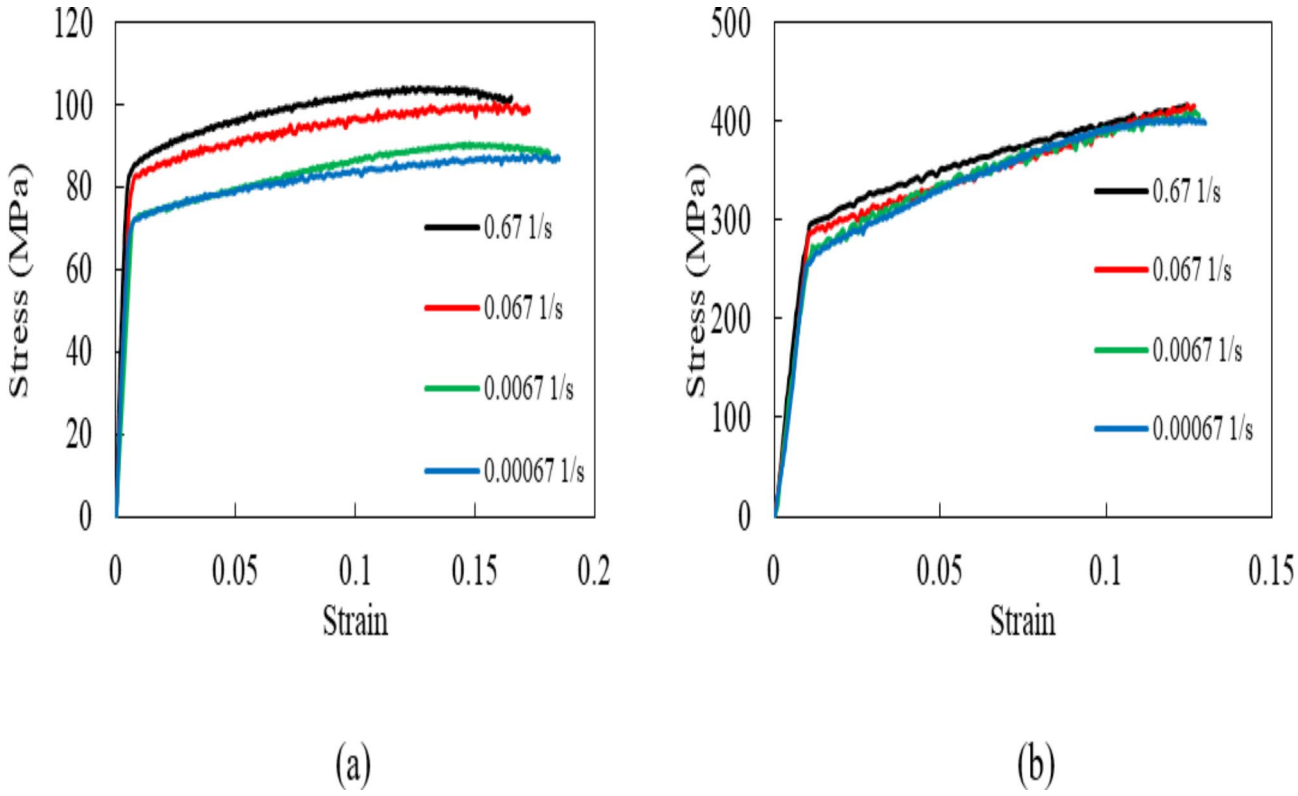

Fig. 6. Stress-strain curves at different strain rate for (**a**) AA 1100 and (**b**) AA 6016-T6 alloys.

experiments, the amount of flow stress (σ) was determined at a specific equivalent plastic strain value ($\bar{\varepsilon}$).This specific value is chosen equal to 0.05. So, the Eq. (2) can be written in following form (Eq. (4)):

$$\sigma = (A + B(0.05)^n)(1 + CLn\dot{\bar{\varepsilon}}) \tag{4}$$

The stress-strain curves at different strain rate and temperatures used to determine the Johnson-Cook constants are presented in Figs. 6 and 7, respectively.

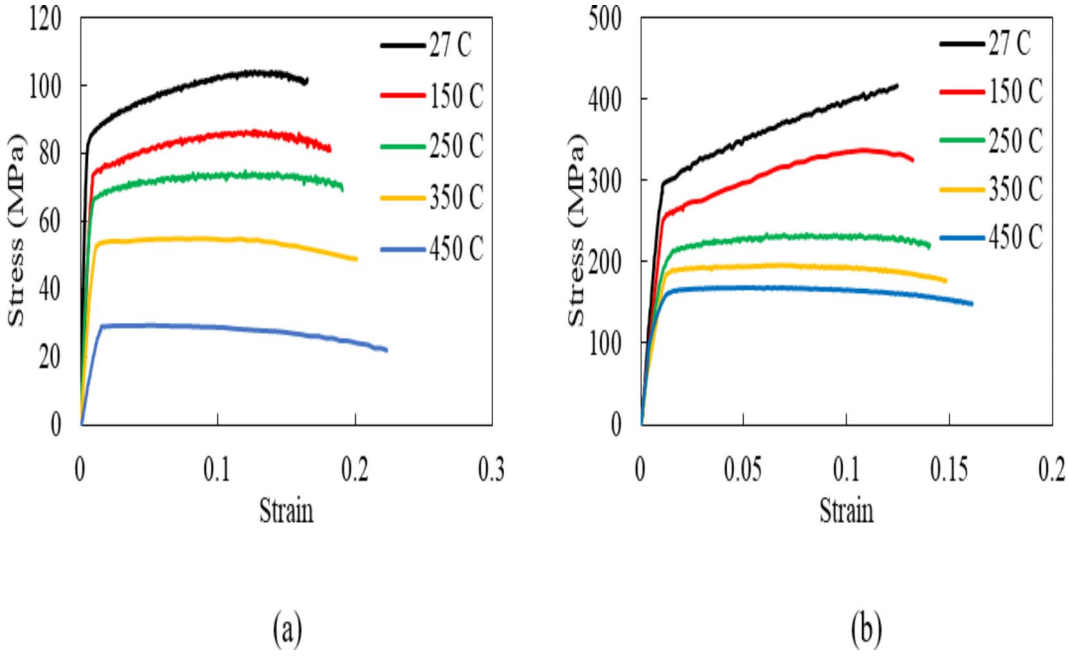

Fig. 7. Stress-strain curves at different temperature for (**a**) AA 1100 and (**b**) AA 6016-T6 alloys.

The points obtained from the tensile tests and the straight lines fitted to them are shown in Fig. 8. Now, it is possible to obtain the value of *C* parameter by determining the slope of these lines. Based on this, the values of this parameter were determined to be 0.021 for AA 1100 and 0.007 for AA 6016-T6.

Similar to what was observed for the strain rate, to determine the *m*- parameter, it is better to rewrite Eq. (2) as Eq. (5):

$$\sigma = (A + B(0.05)^n)(1 - T^{*m}) \tag{5}$$

According to Eq. (5), the values of flow stress at different temperatures were determined from the tensile test, and using the obtained values, the amount of $Ln\,(1 - \sigma/\,(A + B(0.05)^n))$ was calculated. These values are shown in terms of $Ln\,(T^*)$ for aluminum alloys in Fig. 9. Now, a straight line can be fitted on this data, and the slope of this line is actually the same as *m*. With this regard, *m* values for AA 1100 and AA 6016-T6 aluminum alloys were computed to 1.17 and 1.29, respectively. The values of Johnson-Cook material model parameters for aluminum alloys used in the present research work are given in Table 2.

Cold expansion process results

Figure 10 shows a blank specimen and a cold expanded sheet after process performance for AA 1100 and AA 6016-T6 aluminum alloys. The mandrel velocity is considered to 5 mm/min in cold expansion process for both of these samples. All blank samples are similar and only their material is different. The FE results were taken along Line 1 and Line 2 are shown in Fig. 11. This figure demonstrates the contours of x-stress (stress in the longitudinal direction) for AA 1100 alloy and contours of y-stress (stress in the transverse direction) for AA 6016-T6 alloy.

Due to the fact that the thickness of the sheets is much lower than their length and width, it can be said that the condition of plane stress prevails. Also, according to Fig. 11, it can be concluded that x-direction and y-direction correspond to, in turn, the longitudinal and transverse directions. Therefore, it can be said that:

Line 1:

For this line, x-direction is radial direction (σ_r) and y-direction is hoop direction (σ_h). So:

$$\sigma_r = \frac{E}{1-\nu^2}(\varepsilon_x + \nu\varepsilon_y) \text{ and } \sigma_h = \frac{E}{1-\nu^2}(\varepsilon_y + \nu\varepsilon_x) \tag{6}$$

Line 2:

For this line, x-direction is hoop direction (σ_h) and y-direction is radial direction (σ_r). So:

$$\sigma_r = \frac{E}{1-\nu^2}(\varepsilon_y + \nu\varepsilon_x) \text{ and } \sigma_h = \frac{E}{1-\nu^2}(\varepsilon_x + \nu\varepsilon_y) \tag{7}$$

The values of $\varepsilon_x$and $\varepsilon_y$can be read directly from the strain gauges for both lines. The hoop and radial residual stress diagrams for AA 1100 aluminum alloy along line 1 and line 2 are shown in Figs. 12 and 13, respectively. These diagrams have been obtained from practical experiment and numerical simulation.

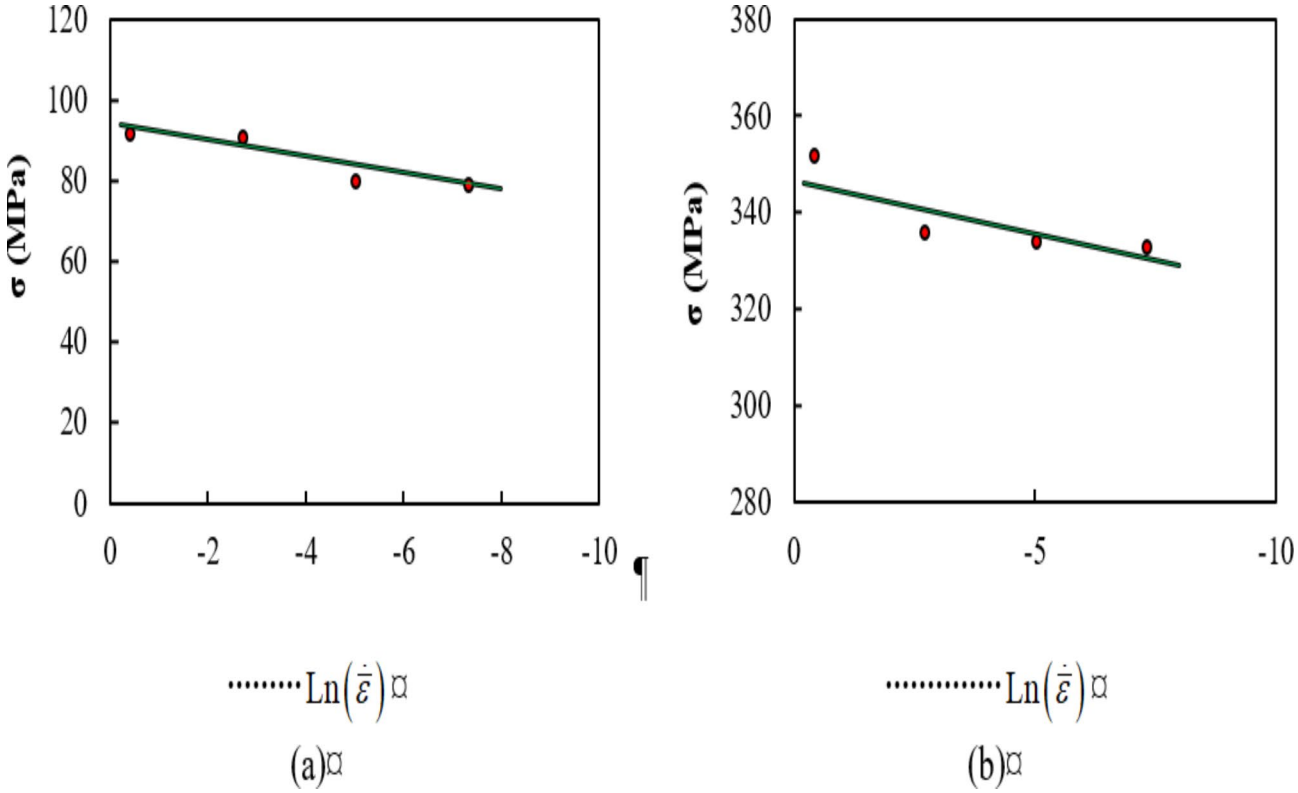

Fig. 8. The amount of flow stress obtained from tensile tests in terms of the logarithmic value of the dimensionless strain rate for (**a**) AA 1100 and (**b**) AA 6016-T6 alloys at $\bar{\varepsilon}=0.05$.

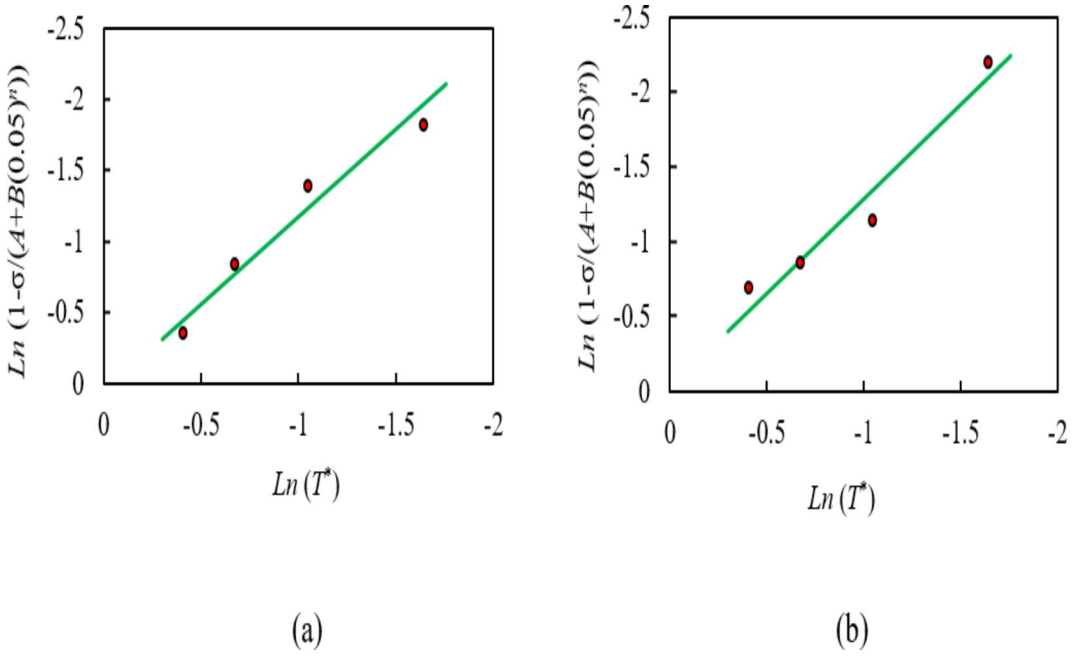

Fig. 9. Values of quantity $Ln\,(1-\sigma/\,(A+B(0.05)^{n}))$ in terms of $Ln\,(T^{*})$ for (a) AA 1100 and (b) AA 6016-T6 aluminum alloys.

Material	A (MPa)	B (MPa)	C	*n*	m
AA 1100	78	62	0.021	0.42	1.17
AA 6016-T6	291	286	0.007	0.63	1.29

Table 2. Parameters of Johnson-Cook material model for AA 1100 and AA 6016-T6 alloys.

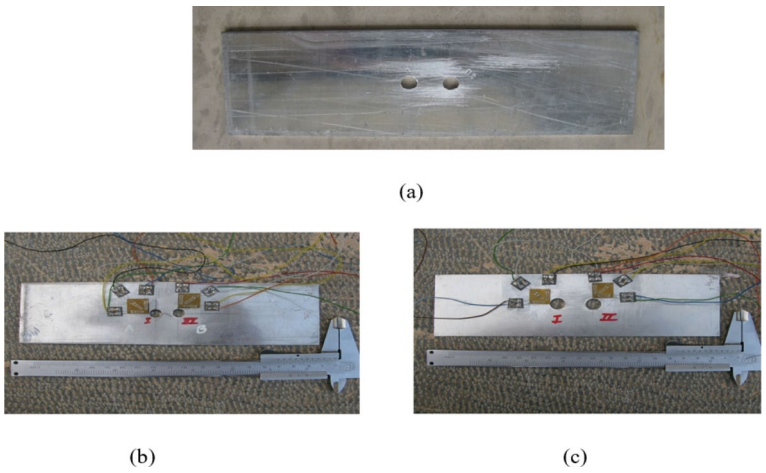

Fig. 10. A view of (**a**) blank sample and a cold expanded sheet after process performance for (**b**) AA1100 and (**c**) AA 6016-T6 alloys.

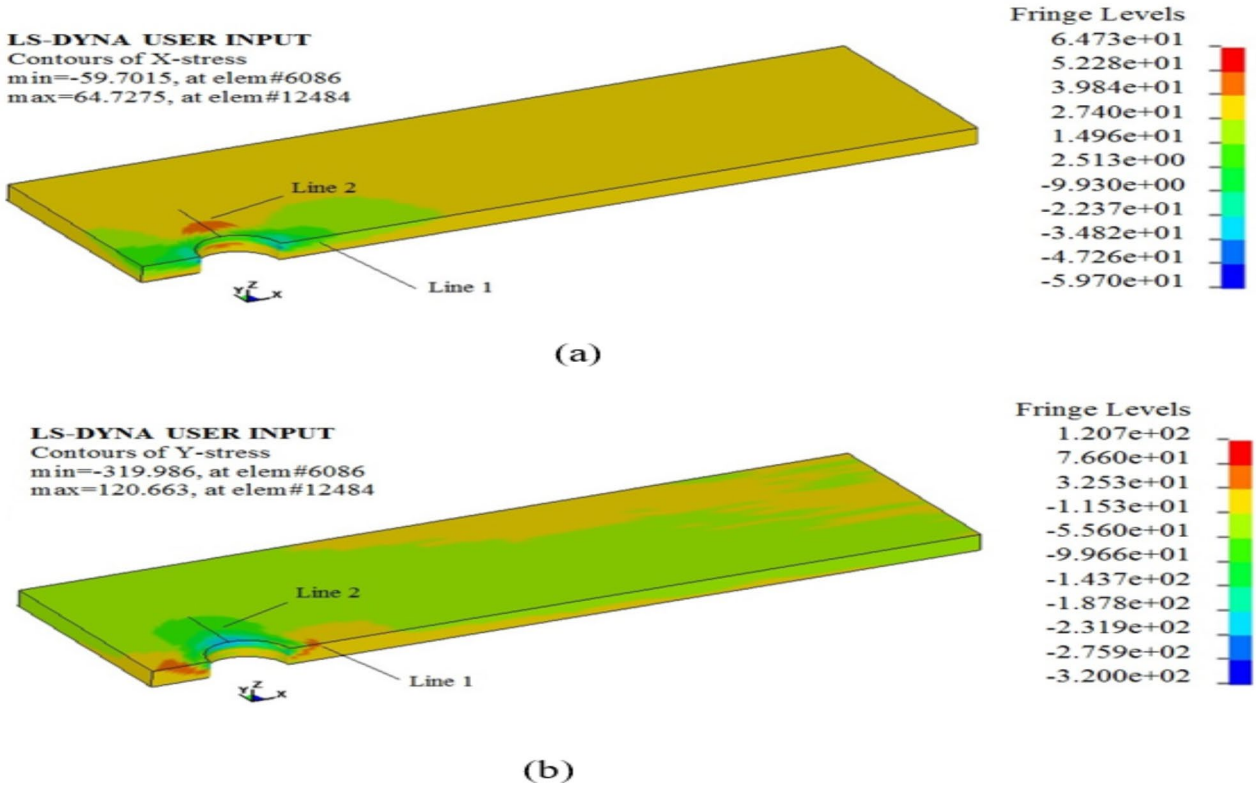

Fig. 11. A view of (**a**) contours of x-stress (stress in the longitudinal direction) for AA 1100 alloy and (**b**) contours of y-stress (stress in the transverse direction) for AA 6016-T6 alloy.

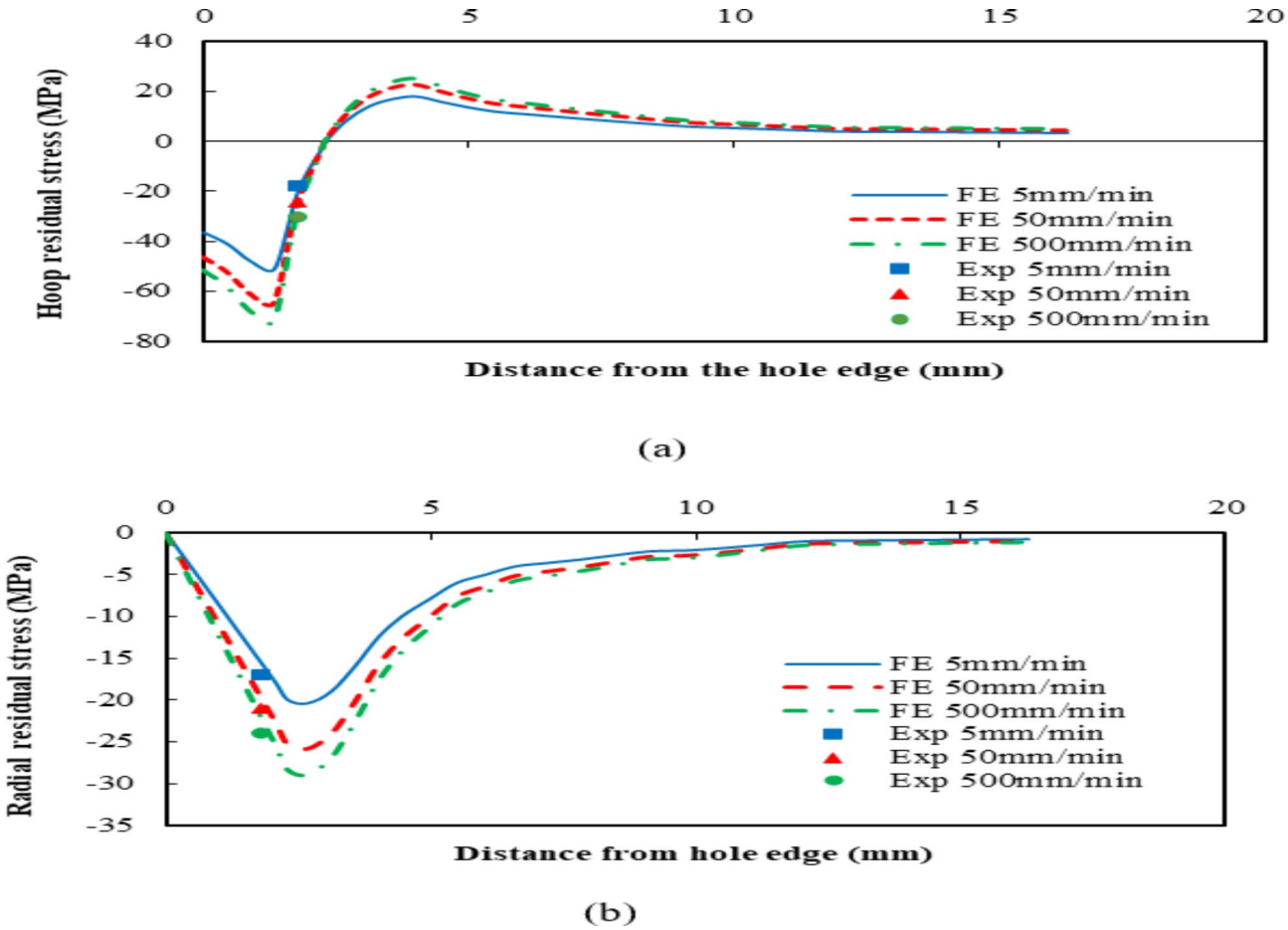

Fig. 12. Residual stress diagrams for AA 1100 aluminum alloy along line 1, (**a**) hoop residual stress and (**b**) radial residual stress.

The comparison of experimental and numerical outcomes demonstrates that there is a good agreement between these results and therefore it can be concluded that the findings obtained from the simulation of the CE process on AA 1100 aluminum alloy are correct and reliable. An important point that can be seen in Figs. 12 and 13 is that in all cases, with the increase in the velocity of the mandrel or the velocity of the CE, the values of the residual stresses increase both on line 1 and on line 2. This issue is especially true in the case of hoop residual stresses that are created at the edge of the sheet hole. Along line 1, by increasing the velocity of the mandrel, the hoop stress created at the edge of the hole can be enhanced (in terms of absolute value) from −36.4 to −51.4 MPa, which is a significant value. The negative sign indicates that the stress is compressive. Also, along line 2, by increasing the velocity of the mandrel, the mentioned stress increases from −41 MPa to -56.3 MPa. Therefore, it can be concluded that by increasing the velocity of the mandrel from 5 to 500 mm/min, the value of hoop residual stress in the longitudinal (line 1) and transverse (line 2) directions are enhanced about 41.2% and 37.3%, respectively. As it can be seen, by increasing the velocity of the mandrel, the values of the residual stress created in the sheet increases. The amount of this increase is significant at the edge of the hole in comparison with other region. Considering that the fatigue failure starts from the surface of the workpiece, it is possible to understand the importance of the amount of stress created on the surface of the hole or its edge. The hoop and radial residual stress curves for AA 6016-T6 aluminum alloy along line 1 and line 2 are presented in Figs. 14 and 15, respectively. According to these figures, there is a good agreement between the numerical and experimental outcomes and therefore the modeling has been done, correctly. By doing the research that was carried out before this study, it was found that if the mandrels enter the holes at the same time, better results are obtained.

Figures 14 and 15 indicate that in AA 6016-T6 aluminum alloy, by intensification in the mandrel velocity, the values of the residual stress in the specimen increases, especially near the edge of the hole. Accordingly, by increasing the mandrel velocity from 5 mm/min to 500 mm/min, the hoop residual stress enhances about 38.1% and 37.6% along the longitudinal direction (line 1) and the transverse direction (line 2), respectively. The obtained results showed that carrying out the CE process causes significant amounts of residual stress to be created around the sheet hole. In addition, if the velocity of the process increases, the values of these residual stresses will increase, and the amount of this enhancement will be higher at the edge of the holes compared to other area. Therefore, it is better to carry out the cold expansion process in materials that are sensitive to the strain rate, at a faster rate, so that larger compressive residual stresses are created at the edge of the holes. In this

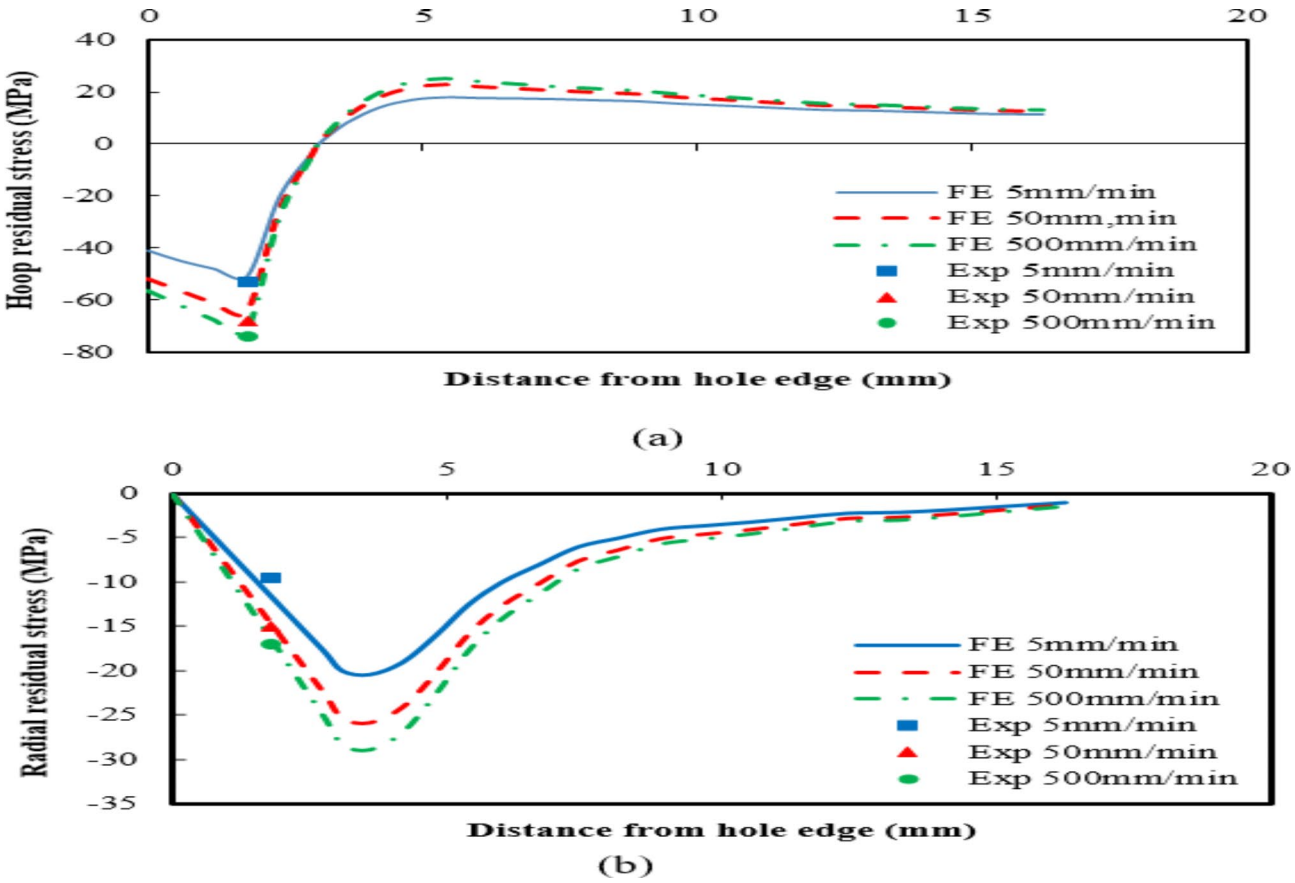

Fig. 13. Residual stress diagrams for AA 1100 aluminum alloy along line 2, (**a**) hoop residual stress and (**b**) radial residual stress.

case, it is possible to increase the sheet's resistance to fatigue failure. Because the failure caused by the fatigue loadings starts from the edge of the hole, making them resistant to the fatigue loads can increases the life of the part, significantly.

Error percentage of numerical results compared to experimental findings for AA 1100 and AA 6016-T6 aluminum alloys are presented in Tables 3 and 4, respectively. These tables show that there are random errors between the obtained numerical and experimental results. The source of these errors can be attributed to measurements noise, modeling assumption, numerical methods, calibration, bias, environmental condition and human factors.

All the diagrams presented for the radial residual stress demonstrated that this stress type is always compressive or zero. The radial residual stress starts from zero at the edge of the hole and reaches zero at a distance from the hole again. Liu et al. used a 3D finite element models to analyze the mandrel force, residual stress distribution and fatigue life of 7075 aluminum alloy after cold expansion operation[2]. Like what was seen in this study, they found that the radial residual stress is always compressive or zero and its value at edge of the hole is zero. Also, the radial residual stress reaches its maximum value at a short distance from the hole and then gradually returns to zero. This trend of variation can be seen in both the longitudinal and the transverse directions for AA 1100 and AA 6016-T6 aluminum alloys. On the other hand, in all cases, the value of hoop residual stress is compressive at the edge of the hole and then it reaches its maximum value in compressive zone as it moves away from the hole. After that, this stress reaches zero and enters the tensile zone. In this zone, it reaches a maximum value with increasing distance from the edge of the hole and then gradually decreases. The hoop residual stress diagrams along line 1 for the entrance face, mid-thickness and the exit face, in AA 1100 aluminum alloy and AA 6016-T6 aluminum alloy are shown in Fig. 16. This Figure indicated that in both alloys, near the hole, the hoop residual stress created in the mid-thickness sheet is higher than the entrance and exit faces. Also, these figures revealed that the stress values in the exit face are higher than the entrance face. The reasons for the lower residual stress created in the entrance face compared to the mid-thickness and exit faces are related to the direction and manner of movement of the mandrel. When the mandrel enters and moves in the hole of the sheets, the material of the workpieces also moves with it towards the inside of the sheet. This issue causes the amount of residual stress created in the entrance sheet to decrease. When the mandrel moves inside the hole of the sheets and moves its material with itself, it actually causes the constraints around the mandrel to change and therefore, the amount of CE created is not the same and uniforms along the thickness of the sheets. In thickness direction, wherever the amount of material is greater, the value of induced CE is also greater, and

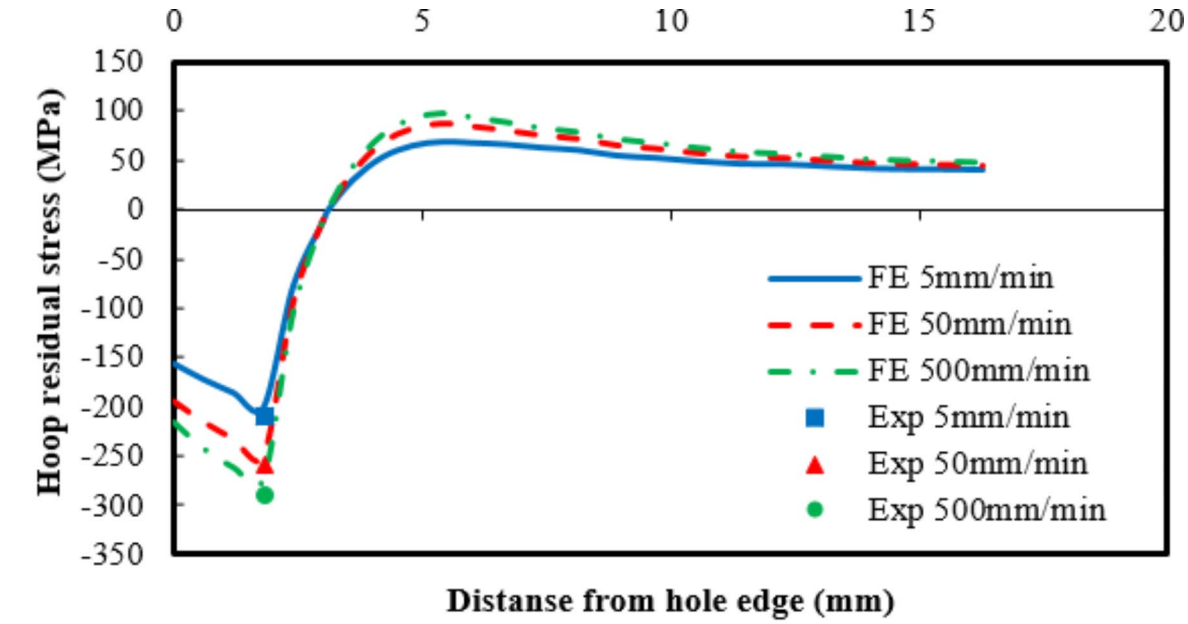

(a)

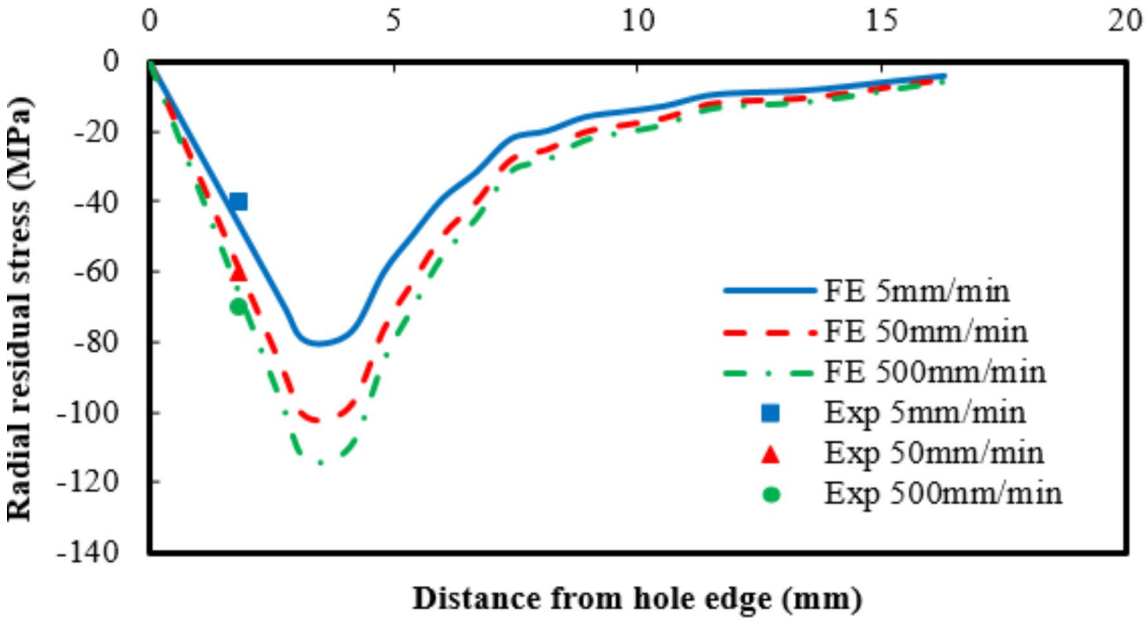

(b)

Fig. 14. Residual stress diagrams for AA 6016-T6 aluminum alloy along line 1, (**a**) hoop residual stress and (**b**) radial residual stress.

therefore, the amounts of residual stresses are bigger. So, the induced residual stress in the mid-thickness of the sheet is greater than the entrance face and the exit face. Nigrelli and Pasta[37] developed a three-dimensional finite-element simulation for a split-sleeve cold expansion process in order to determine the residual stress field around an expanded hole. By using this study, they realized that the magnitude of compressive hoop residual stresses on the entrance and the exit faces are lower than the stresses on the mid-thickness. Also, Yucan et al.[38] investigated on the cold expansion technology of connection holes in aircraft structures. They finite element

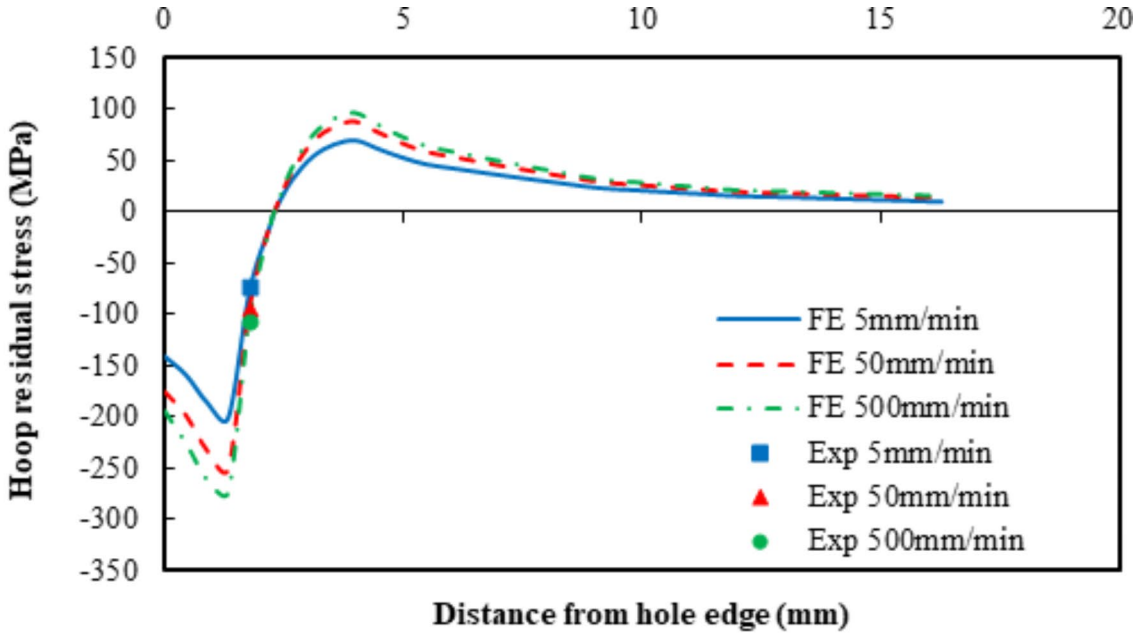

(a)

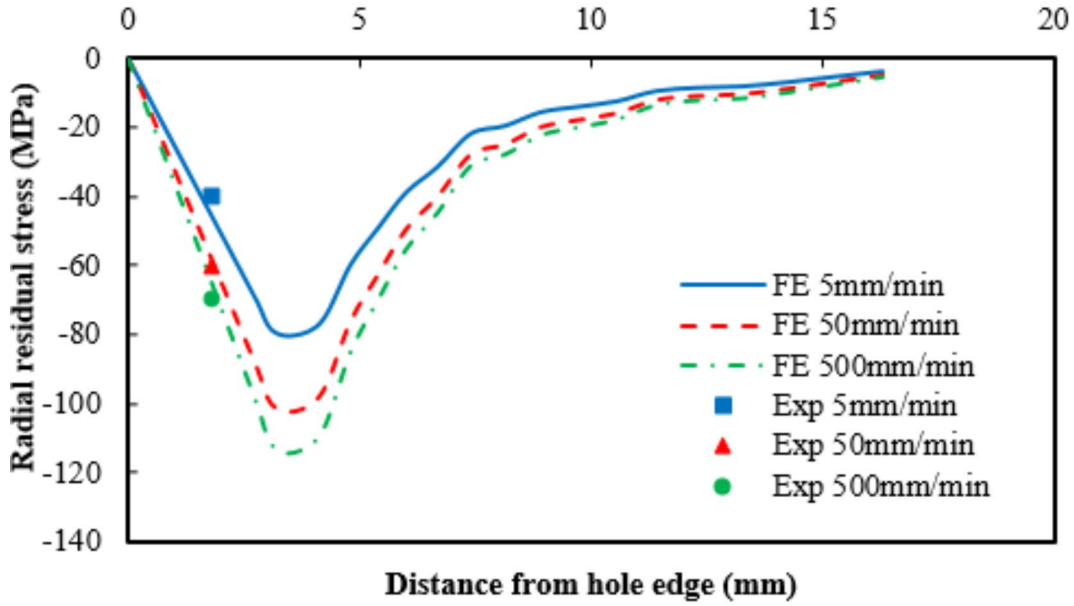

(b)

Fig. 15. Residual stress diagrams for AA 6016-T6 aluminum alloy along line 2, (**a**) hoop residual stress and (**b**) radial residual stress.

results show that during the hole cold expansion process, the residual compressive stress of the hole edge exhibits grades across the thickness with the least amount of residual compressive stress at the tool entrance face, the largest amount of residual compressive stress in the mid-bore, and good residual compressive stress at the tool exit face. As mentioned before, fatigue failure often starts from the surface of the hole, and therefore, the amount of stress on the surface of the hole is of special importance. In AA 1100 aluminum alloy, the hoop residual stress values created on the surface of the hole in the entrance face, exit face and the mid-thickness of the thickness

Line 1						Line 2					
Hoop			Radial			Hoop			Radial		
5 mm/min	50 mm/min	500 mm/min	5 mm/min	50 mm/min	500 mm/min	5 mm/min	50 mm/min	500 mm/min	5 mm/min	50 mm/min	500 mm/min
−10.0	−2.0	6.2	10.2	7.2	9.4	3.9	4.6	2.8	−17.8	2.0	3.0

Table 3. Error percentage of numerical results compared to experimental findings for AA 1100 alloy.

Line 1						Line 2					
Hoop			Radial			Hoop			Radial		
5 mm/min	50 mm/min	500 mm/min	5 mm/min	50 mm/min	500 mm/min	5 mm/min	50 mm/min	500 mm/min	5 mm/min	50 mm/min	500 mm/min
4.4	3.2	5.9	6.9	−6.7	−5.1	−4.4	1.45	3.6	−12.2	3.5	7.9

Table 4. Error percentage of numerical results compared to experimental findings for AA 6016-T6 alloy.

are equal to 51.4 MPa, 71.5 MPa and 86.7 MPa, respectively. Also, these values for AA 6016-T6 aluminum alloy are computed to −215.3 MPa, −290.9 MPa and −315.2 MPa respectively. Figure 16 indicated that the size of the zone where the compressive hoop residual stress occurs in the entrance face is greater than this size in the exit face. Also, the mentioned size in the exit side is more than this size in the mid-thickness. For example, the size of the compressive hoop residual stress in AA 6016-T6 aluminum alloy along line 1 is 3.1 mm, 2.7 mm, and 2.4 mm for the entrance, exit, and mid-thickness faces, respectively. The cause of this phenomenon is the presence of more material in the mid-thickness sheet compared to the other two faces and the presence of more material in the exit sheet than the entrance sheet, which was transferred to it along with the mandrel. In general, the sheet material act as a constraint, which increases the amount of residual stress created in the sheets, and on the other hand, reduces the size of the zone where the compressive hoop residual stress is created. Due to the fact that the residual stress created in the entrance face is relatively low, therefore, the failure phenomenon starts from this face. Thus, sometimes to eliminate this defect, the CE process is done twice, and the second time the process is done in reverse and the mandrel enters from the other side of the sheet. So, the face that was the entrance face in the first time will be the exit face in the second time. The current research showed that in the CE process, the entrance face is the weakest in direction of thickness. Figures 12, 13, 14 and 15 also demonstrated that near the edge of the holes, the amount of hoop residual stress created in the sheet and consequently, the resistance of the sheet in the transverse direction is lower than the longitudinal direction. So, when the fatigue load is applied to such a sheet, the fatigue failure starts from the entrance face and continues in the transverse direction. This has been confirmed, experimentally.

Conclusions

In the present research work, the hoop and radial residual stresses that arise in the cold expansion (CE) process have been investigated. The effects of the mandrel velocity in this process on the stresses created in two materials, namely AA 6016-T6 and AA 1100 aluminum alloys, have been studied, experimentally and numerically. The main results obtained from present research can be summarized as follows:

1. 1. For the special conditions that existed in the current study and among the velocities that were considered in this research, the most appropriate value of mandrel velocity is 500 mm/min to perform the cold expansion process on AA 1100 and AA 6016-T6 aluminum alloys because it produces the most useful residual stresses.
2. 2. The values of the residual stresses created in sheets made of AA 1100 and AA 6016-T6 aluminum alloys in the CE process depend on the velocity of the process. By increasing the velocity of the mandrel, it is possible to reach higher values of the residual stresses in the hoop and radial directions of the sheet hole.
3. 3. At the edge of the sheet's holes, by intensifying the velocity of the mandrel from 5 mm/min to 500 mm/min, it is conceivable to enhance the hoop residual stress in the longitudinal and transverse directions about 41.2% and 37.3% in AA 1100, and 38.1% and 37.6% in AA 6016-T6 aluminum alloys, respectively.
4. 4. Due to the existence of material constraints and the movement of the sheet material with the mandrel, the amount of hoop residual stress created in the mid-thickness is more than the exit face and in the exit face is also more than the entrance face. For example at the edge of the hole in AA 1100 aluminum alloy, these stresses are −86.7 MPa, −71.5 MPa and −51.4 MPa, respectively. Also, these values for AA 6016-T6 aluminum alloy are, in turn, −315.2 MPa, −290.9 MPa and − 215.3 MPa.
5. 5. Unlike the amounts of the hoop stresses at the hole edge, because of the existence of material constraints and the movement of the sheet material with the mandrel, the size of the compressive residual stress zone created in the mid-thickness is more than the this zone size of exit face and in the exit face is also greater than the entrance face.

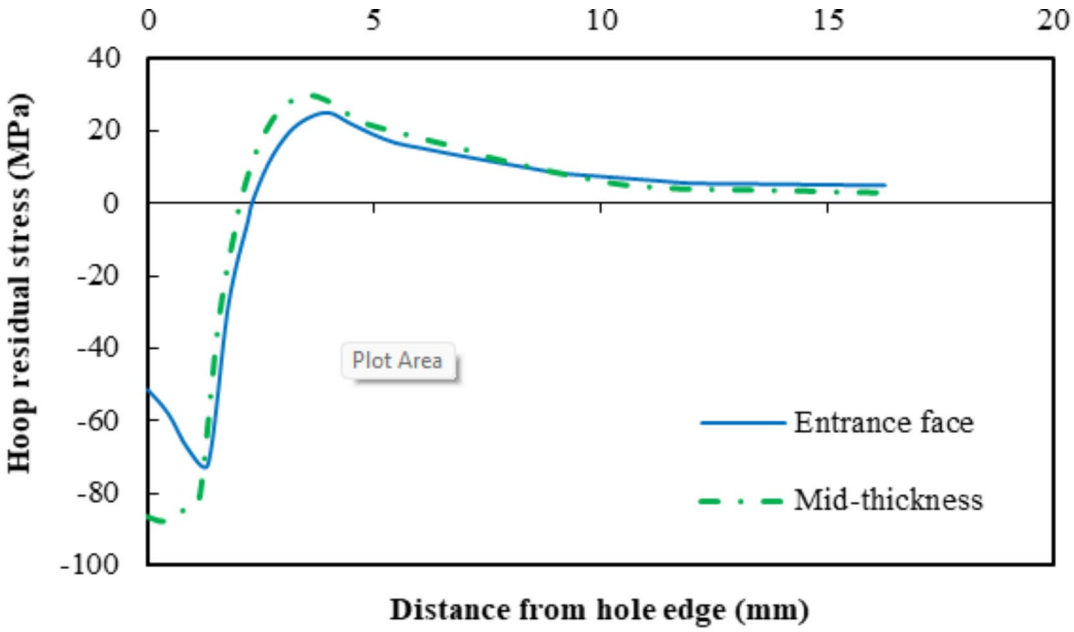

(a)

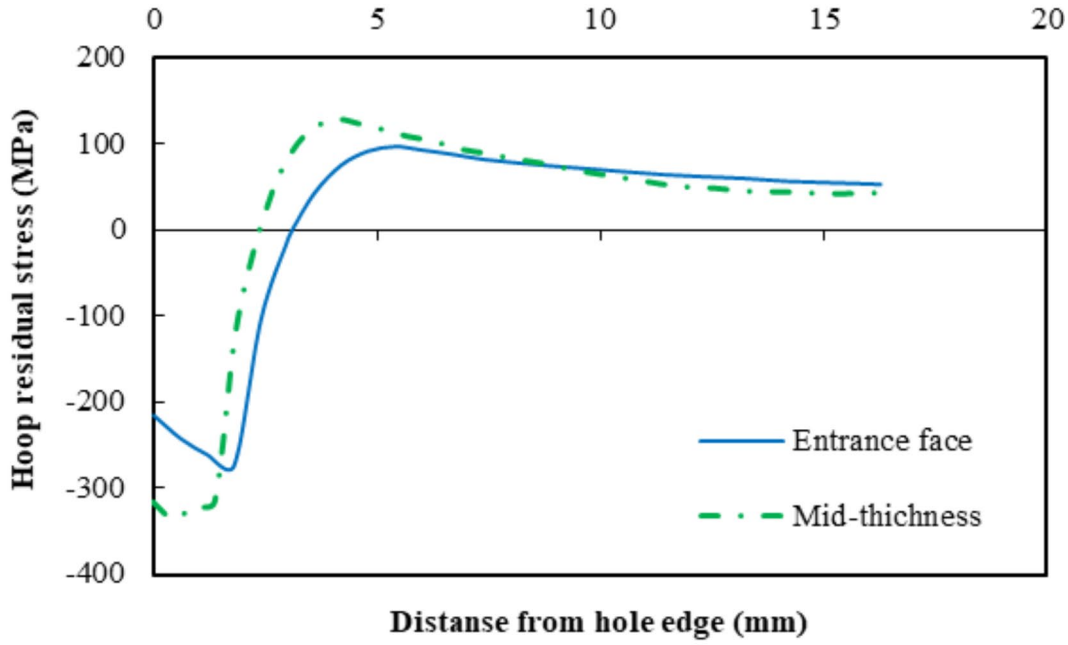

(b)

Fig. 16. The hoop residual stress diagrams along line 1 for the entrance face, mid-thickness and the exit face, for (**a**) AA 1100 aluminum alloy and (**b**) AA 6016-T6 aluminum alloy.

Data availability

The datasets generated and analyzed during the current study are available from the corresponding author on reasonable request.

Received: 20 May 2024; Accepted: 29 October 2024
Published online: 07 November 2024

References

1. Pucillo, G. P., Carrabs, A., Cuomo, S., Elliott, A. & Meo, M. Cold expansion of rail-end-bolt holes: finite element predictions and experimental validation by DIC and strain gauges. *Int. J. Fatigue*. **149**, 106275 (2021).
2. Liu, K. et al. Finite element Simulation of the Cold expansion process with Split Sleeve in 7075 aluminum Alloy. *J. Institution Eng. (India): Ser. C*. **102**, 361–374 (2021).
3. Shahriary, P. & Chakherlou, T. N. Investigating the effect of cold expansion on frictional force evolution during fretting fatigue tests of AL2024-T3 plates. *Int. J. Mech. Sci.* **135**, 146–157 (2018).
4. Chinara, M., Paul, S. K., Chatterjee, S. & Mukherjee, S. Effect of Planar Anisotropy on the hole expansion ratio of Cold-rolled DP 590 steel. *Trans. Indian Inst. Met.* **75**, 535–543 (2021).
5. Faghih, S., Shaha, S. K., Behravesh, S. B. & Jahed, H. Split sleeve cold expansion of AZ31B sheet: microstructure, texture and residual stress. *Mater. Des.* **186**, 108213 (2020).
6. Khan, M. A. & Masanta, M. Fabrication of AISI 434L Stainless Steel Thin Wall Structures by TIG-Aided Powder Bed Fusion Arc Additive Manufacturing: Evaluation of Metallurgical Characteristics and Mechanical Properties. *J. Mater. Eng. Perform.* 1–12. https://doi.org/10.1007/s11665-024-09874-w (2024).
7. Salami, K., Abdi Behnagh, R., Agha Mohammad Pour, M. & Brighenti, R. Numerical study of refill friction stir spot welding of dissimilar metallic materials using smoothed particle hydrodynamics (SPH). *Acta Mech.* **235**(10), 6321–6339. https://doi.org/10.1007/s00707-024-04047-1 (2024).
8. Mathieu, S., Podor, R., Emo, M., Hunault, L., Vilasi, M., Cormier, J., & Pedraza, F. Short-Term Oxidation in HT-SEM of the Pt-Containing TROPEA Single Crystal Ni-Based Superalloy from 680 to 1000°C. *High Temperature Corrosion of Materials* **101**(5), 1211–1223. https://doi.org/10.1007/s11085-024-10272-9 (2024).
9. Sharma, R. et al. Distinct metabolic requirements regulate B cell activation and germinal center responses. *Nat. Immunol.* **24**, 1358–1369 (2023).
10. Shuai, H. et al. Effect of hole cold expansion on fatigue performance of corroded 7B04-T6 aluminium alloy. *Int. J. Fatigue*. **126**, 210–220 (2019).
11. Wang, Y., Fu, B., Nie, L. & Sun, T. Fatigue nucleation site of cold expansion hole varying as fatigue load level varies. *SN Appl. Sci.* **1**, 867 (2019).
12. Abubakar, A. A. et al. Evaluation of residual stress in thick metallic coatings using the combination of hole drilling and micro-indentation methods. *J. Mater. Res. Technol.* **20**, 867–881 (2022).
13. Sun, J. & Dilger, K. Influence of initial residual stresses on welding residual stresses in ultra-high strength steel S960. *J. Manuf. Process.* **101**, 259–268 (2023).
14. La Fé-Perdomo, I., Ramos-Grez, J. A., Jeria, I., Guerra, C. & Zambrano-Robledo, P. Simultaneous optimization of Surface Roughness and Mechanical properties of 316L Produced by LB–PBF using Grey Relational Analysis complemented by residual stress analysis. *Arab. J. Sci. Eng.* **49**, 2285–2298 (2024).
15. Zhu, X., Wang, X. & Wu, H. Calculation method and analysis of residual stress in the strip bending roller straightening process. *Sci. Rep.* **14**, 9149 (2024).
16. ASTM International Committee E-28 on Mechanical Testing. Standard Test Methods for Tension Testing of Metallic Materials. (2021).
17. Dorfmann, L. & Ogden, R. W. The effect of residual stress on the stability of a circular cylindrical tube. *J. Eng. Math.* **127**, 9 (2021).
18. Muhayat, N. et al. Effect of Zn Addition on the Hardness of Friction Stir Processed Aluminium 1100. In: Salim MA, Khashi'ie NS, Chew KW, Photong C, editors. Proceedings of the 9th International Conference and Exhibition on Sustainable Energy and Advanced Materials. Singapore: Springer Nature Singapore. 95–101. (2024).
19. Abedinimanesh, P., Hazinia, F. & Ganjiani, M. Influence of plastic anisotropy and stress state on damage evolution and fracture behavior of aluminum 1100. *J. Brazilian Soc. Mech. Sci. Eng.* **45**, 34 (2023).
20. Prakash, M., Kanthababu, M. & Rajurkar, K. P. Investigations on the effects of tool wear on chip formation mechanism and chip morphology using acoustic emission signal in the microendmilling of aluminum alloy. *Int. J. Adv. Manuf. Technol.* **77**, 1499–1511 (2015).
21. Venkateshwar Reddy, P. & Veerabhadra Reddy, B. Effect of tube material and heat treatment temperatures on tube formability during tube hydroforming process. *J. Institution Eng. (India): Ser. C*. **101**, 991–998 (2020).
22. Abedinimanesh, P., Hazinia, F. & Ganjiani, M. Influence of plastic anisotropy and stress state on damage evolution and fracture behavior of aluminum 1100. *J. Brazilian Soc. Mech. Sci. Eng.* **45**, 34 (2022).
23. Sargeant, D. et al. Effect of pre-strain on springback behavior after bending in AA 6016-T4: experiments and crystal plasticity modeling. *Int. J. Solids Struct.* **283**, 112485 (2023).
24. Xi, R., Xie, J. & Yan, J-B. Evaluations of low-temperature mechanical properties and full-range constitutive models of AA 5083-H112/6061-T6. *Constr. Build. Mater.* **411**, 134520 (2024).
25. Engler, O., Marioara, C. D., Aruga, Y., Kozuka, M. & Myhr, O. R. Effect of natural ageing or pre-ageing on the evolution of precipitate structure and strength during age hardening of Alâ€Mgâ€Si alloy AA 6016. *Mater. Sci. Engineering: A*. **759**, 520–529 (2019).
26. Gattmah, J., Ozturk, F. & Orhan, S. Experimental and finite element analysis of residual stresses in cold tube drawing process with a fixed mandrel for AISI 1010 steel tube. *Int. J. Adv. Manuf. Technol.* **93**, 1229–1241 (2017).
27. Gattmah, J., Ozturk, F., Shihab, S. K. & Orhan, S. Influencing the residual stresses in tubes drawn with a floating plug by changing tool parameters. *J. Brazilian Soc. Mech. Sci. Eng.* **44**, 298 (2022).
28. Geng, H., Xu, X., Cao, Q., Lai, Z. & Li, L. Improving the fatigue performance of AZ31 sheet with hole via electromagnetic cold expansion process. *Int. J. Adv. Manuf. Technol.* **120**, 5057–5071 (2022).
29. Pucillo, G. P., De Vita, G. & Fedeli, E. Fatigue crack growth rate dependency on cold expansion degree in railway steel. *Procedia Struct. Integr.* **39**, 700–710 (2022).
30. Faghih, S., Behravesh, S. B., Kumar Shaha, S. & Jahed, H. Effect of split sleeve cold expansion on fatigue and fracture of rolled AZ31B magnesium alloy. *Theoret. Appl. Fract. Mech.* **123**, 103715 (2023).
31. Gattmah, J., Ozturk, F. & Orhan, S. A new development of measurement technique for residual stresses generated by the cold tube drawing process with a fixed mandrel. *Int. J. Adv. Manuf. Technol.* **108**, 3675–3687 (2020).
32. Su, R. et al. Investigation on fatigue failure of split-sleeve cold expansion holes of 7075-T651 aluminum alloy. *Mater. Today Commun.* **35**, 106290 (2023).
33. Chen, Z., Peng, C. & Zuo, Y. Effects of lubrication conditions on cold expansion fatigue strengthening performances of titanium alloy open hole structures. *Ocean Eng.* **310**, 118733 (2024).
34. Deng, W. et al. Steel–aluminum screw–thread pair tightening mechanism and fastening axial force conversion efficiency. *Results Eng.* **22**, 102049 (2024).
35. Zhang, R., Chen, L., Xie, K., Liu, K. & Wu, Z. Compression properties and constitutive model of short glass fiber reinforced poly-ether-ether-ketone (PEEK). *Sci. Rep.* **13**, 19206 (2023).
36. Pourhamid, R. & Shirazi, A. A comprehensive damage criterion in tube hydroforming. *Proc. Institution Mech. Eng. Part. B: J. Eng. Manuf.* **235**, 417–430 (2021).
37. Nigrelli, V. & Pasta, S. Finite-element simulation of residual stress induced by split-sleeve cold-expansion process of holes. *J. Mater. Process. Technol.* **205**, 290–296 (2008).

38. Fu, Y., Ge, E., Su, H., Xu, J. & Li, R. Cold expansion technology of connection holes in aircraft structures: a review and prospect. *Chin. J. Aeronaut.* **28**, 961–973 (2015).

Author contributions

S. Y: Conceptualization, Project administration, Supervision, Writing- Original draft, Formal analysis, Data curation.A. Sh: Methodology, Investigation, Software, Resources.All authors reviewed the manuscript.

Declarations

Competing interests

The authors declare no competing interests.

Additional information

Correspondence and requests for materials should be addressed to S.Y.

Reprints and permissions information is available at www.nature.com/reprints.

Publisher's note Springer Nature remains neutral with regard to jurisdictional claims in published maps and institutional affiliations.